Design and implementation of low-power low-cost quasi steady-state magnetoplasmadynamic propulsion using Ar-He and N_2-He gas mixtures

C.A. Barry Stoute

Department of Earth and Space Science and Engineering,
Lassonde Engineering,
York University,
Toronto, Ontario, M3J1P3, Canada
Email: stoute.barry@gmail.com

Abstract: Current miniature plasma propulsion technologies use ion or Hall propulsion to provide thrust for miniature satellites. The problem with ion and Hall thrusters is the low thrust-to-power ratio (30 mN/kW–50 mN/kW), and it is not enough for high-speed manoeuvres in deep-space missions. Alternatively, magnetoplasmadynamic propulsion provides higher thrust to miniature satellites than ion thrusters without the increase in mass. Magnetoplasmadynamic propulsion is a technology that the plasma is accelerated electromagnetically. This research investigates the design and performance of a low-cost magnetoplasmadynamic thruster built for micro and nanosatellites. Gas mixtures are tested in this research to observe any improvement in the overall performance. The gases used in the thruster are pure helium, nitrogen and argon; with gas mixtures of 50% helium – 50% nitrogen and 50% helium – 50% argon. The specific impulse, impulse bit, thrust efficiency and thrust-weight ratios of 50% helium – 50% nitrogen are 801 seconds, 6.29 μN·s, 19.8% and 15.72 mN/kg, respectively.

Keywords: magnetoplasmadynamics; MPD; propulsion; electric; space; astronautics; plasma.

Reference to this paper should be made as follows: Stoute, C.A.B. (2021) 'Design and implementation of low-power low-cost quasi steady-state magnetoplasmadynamic propulsion using Ar-He and N_2-He gas mixtures', *Int. J. Aerospace System Science and Engineering*, Vol. 1, No. 1, pp.20–34.

Biographical notes: C.A. Barry Stoute received his PhD in Space Engineering and Postdoctoral Fellowship in Energy Systems Engineering, and his work is on plasma propulsion and power generation. He has over seven years of experience working in thermal vacuum chambers, power electronics, plasma generation and power and propulsion. He also has three years of experience in optomechanical engineering. He has knowledge in quantum and particle physics. He is responsible for the project, alongside with his PhD Supervisor, Dr. Brendan M. Quine.

1 Introduction

Electrostatic propulsion is a technology in which the ions are accelerated by an electric field. Ion and Hall thrusters are the two most common types of electrostatic thrusters (Goebel and Katz, 2008). They have been implemented in full-size satellites for deep space missions, and currently, there is research on the miniaturisation of such technology. The main concern of ion and Hall thrusters is the low thrust-to-power ratio (Goebel and Katz, 2008; Sutton and Biblarz, 2010) in respect to other electric and chemical thrusters. This may be problematic when high-thrust manoeuvres are necessary if encountering objects in low-Earth orbit, like other satellites.

Electromagnetic propulsion has a relatively higher thrust than electrostatic propulsion under the same power input, which can provide the necessary thrust. An established electromagnetic propulsion technology which is used in the space industry is the pulse-plasma thruster. This thruster ablates a solid propellant, such as PTFE, using a spark plug for ionisation and the propellant is accelerated by the current from the capacitor (Jahn, 1968). Other magnetoplasmadynamic (MPD) thrusters, such as the variable specific impulse magnetorocket (VASIMR), which uses 200 kW of power for 0.5 N of thrust (Chang Díaz et al., 1999).

This paper focuses on a low-power low-cost gas-fed MPD thruster for nanosatellites (wet mass including electronics < 10 kg). The gas is ionised and accelerated by a single power source. This research is a part of a dual-mode hybrid thruster in which both ion and MPD thrusters are operating in parallel (Stoute, 2013). It focuses on maximising the performance peak efficiency by recycling any energy loss coming from the system; thus, the MPD thruster was design with a converging-diverging nozzle where the solenoid from an RF circuit reheats the plasma (Stoute, 2013). In this paper, the solenoid was inactive; however, the mass of the solenoid is negligible in the total mass of the thruster. Figure 1 illustrates the outline of the MPD thruster in this paper.

Figure 1 MPD thruster with the nozzle

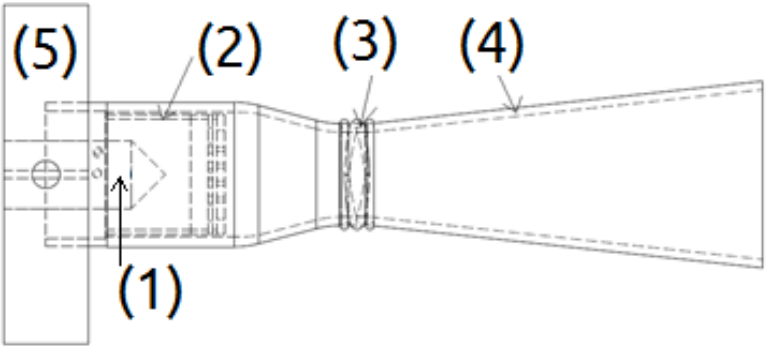

Notes: (1) – cathode tip; (2) – anode cylinder; (3) – reheating solenoid (inactive); (4) – nozzle; (5) – thruster support.

The MPD thruster is run in a quasi-steady state that uses capacitors and a power supply to provide both the necessary voltage and current. This is a part due to the requirement of the thruster to be a minimal-cost equipment. The cost significantly reduces by using innovative techniques. This is discussed in detail in Section 3.2 (Martinez-Sanchez, 2004;

Domonkos et al., 1995). The propellants of the MPD thruster are comprised of gas mixtures. The gas mixtures are argon-helium and nitrogen-helium. The use of such mixtures investigates the alternative use for pure gases.

The paper first discusses the propulsion theory of the thruster. The propulsion theory section discusses the nozzle theory of the thruster and the MPD propulsion theory. The experiment section discusses the methodology and results of the thruster. The discussion section focuses on the analysis of the findings and performance comparisons. The last section discusses the conclusion made from this paper.

2 Propulsion theory

The propulsion theory discusses the nozzle theory and MPD propulsion theory. The nozzle theory discusses the resulting pressure and area ratios from the heat capacity ratio and the Mach number of the propellant. These calculations yield the results for the exhaust velocity, thrust, and the specific impulse (Sutton and Biblarz, 2010).

The exhaust velocity is the speed and direction of the particle as it exits the nozzle. The exhaust velocity vex is given by Sutton and Biblarz (2010):

$$v_{ex} = \sqrt{T \cdot \frac{R}{M} \cdot \frac{2\gamma}{\gamma+1} \cdot \left(1 - \left(\frac{P_e}{P_t}\right)^{\frac{(\gamma-1)}{\gamma}}\right)}, \tag{1}$$

where T, R, M, γ, P_e, and P_t are the temperature of the plasma, universal gas constant (8,314 J·kmol^{-1}·K^{-1}), the atomic mass (kg/kmol), heat capacity ratio, exhaust and throat pressures respectively. Given the exhaust velocity, the thrust is (Sutton and Biblarz, 2010):

$$F_{thrust} = \dot{m} \cdot v_{ex}, \tag{2}$$

where $\dot{m}$ and v_{ex} are the mass flow rate and the exhaust velocity (Sutton and Biblarz, 2010). Note that the exhaust velocity is a scalar quantity.

MPD propulsion uses magnetic fields to accelerate the plasma. In a self-induced field MPD thruster, the force is found by the Maecker's formula. Maecker's formula is derived from the Lorentz force (Jahn, 1968):

$$F_{Maecker} = \frac{\mu_0 I^2}{4\pi} \cdot ln\left(\frac{r_a}{r_c} + C_{tip}\right), \tag{3}$$

where μ_0, I, r_a, and r_c are the permeability of free space, current, radii of the anode and cathode of the coaxial thruster, respectively. The current, I, is the total current which come across from the cathode to the anode, through the plasma. The constant, C_{tip}, is a value which ranges between 0 and 0.75, depending on the shape of the cathode and arc attachment of the area (Jahn, 1968).

Specific impulse is defined as the exhaust velocity of the propellant divided by the Earth's gravitational acceleration at sea level; or, the amount of thrust divided by the accelerated mass flow rate of the propellant:

$$I_{sp} = \frac{v_{ex}}{g_0} = \frac{F_{thrust}}{\dot{m} g_0}, \tag{4}$$

where F_{thrust} is the total thrust from the nozzle and the MPD thruster (Jahn, 1968; Sutton and Biblarz, 2010).

The exhaust velocity from the thruster reaches its peak velocity when the gas is fully ionised (Martinez-Sanchez, 2004). A peak velocity is achieved when the kinetic energy is equal to the ionisation energy of the particle. This velocity is called Alfvèn's critical velocity:

$$v_{critical} = \sqrt{2 \cdot \frac{E_i}{m_i}} \cdot \tag{5}$$

Impulse bit is the amount of thrust over a period of time, or the change in momentum. This is analysed when the thruster is running in quasi-steady state (Domonkos et al., 1995; Guarducci et al., 2011):

$$I_{bit} = \int_{0.}^{t} F_{thrust}(t) \cdot dt = g_0 I_{sp} \dot{m} \Delta t, \tag{6}$$

where $I(t)$ is the time-dependent current inside the plasma, and Δt is the period of the pulse.

3 Thruster design

3.1 Thruster

The MPD thruster is a coaxial design which the outer cylinder (anode) is made of brass, and the inner cylinder (cathode) is made of aluminium. The cathode has a sharp tip to increase the thrust such that the value of C_{tip} from equation (4) is 0.75. The effective dimensions, where the plasma is generated and accelerated, of the anode are 10 mm in length, and 13 mm in diameter. The propellant is inserted radially in the cavity to ensure the propellant is diffused. The cathode, inner cylinder, is made of aluminium with a pointed tip. The effective dimensions of the cathode are 9 mm in length, and 8 mm in diameter. Figures 2(a) and 2(b) show the illustrations of the electrodes. All the measurements are in millimetres and degrees.

The nozzle is a standard converging-diverging conical nozzle. The exhaust diameter is 20 mm and the throat diameter is 10 mm. The length of the diffuser is 46 mm. The throat of the nozzle has the length of 3 mm. Figure 3 shows the mechanical drawing of the nozzle.

Figure 2 (a) The anode, all dimensions are in millimetres (b) The cathode, all dimensions are in millimetres

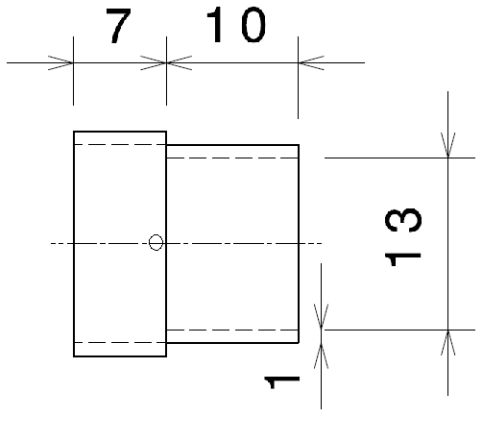

(a)

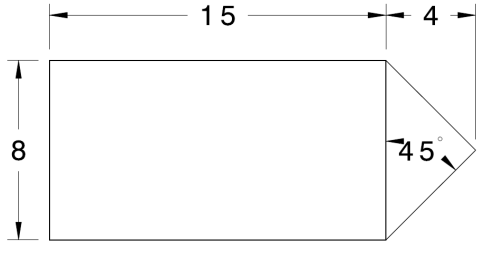

(b)

Figure 3 Mechanical drawing of the glass nozzle

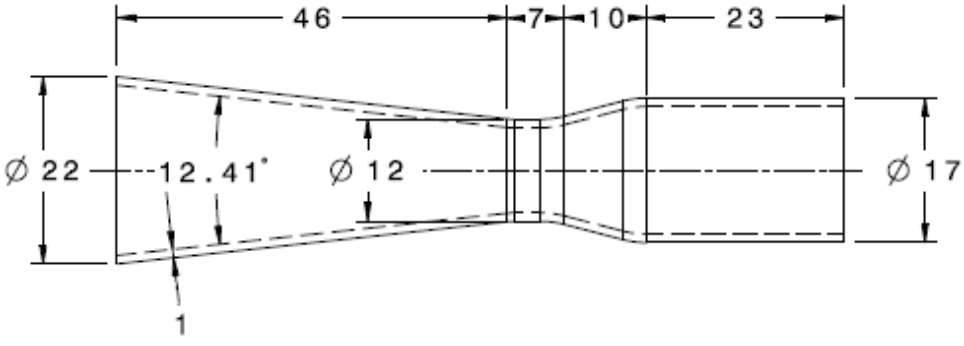

Note: All dimensions are in millimetres.

3.2 Circuit design

The MPD thruster operates in a quasi-steady state via capacitors. The electronic configuration of the thruster is shown in Figure 4.

Figure 4 Electronic configuration of the EM thruster

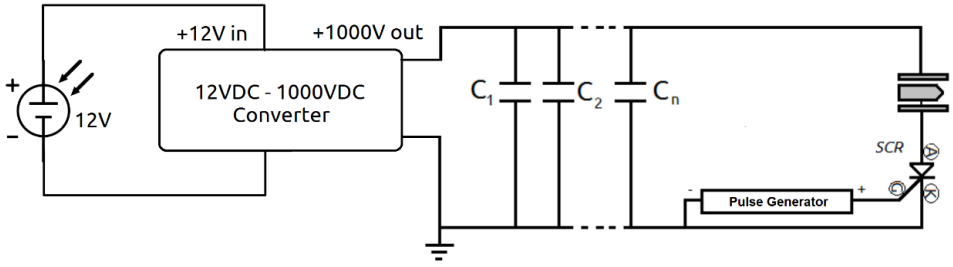

Figure 5 Current vs. time resulting from equation (7) (see online version for colours)

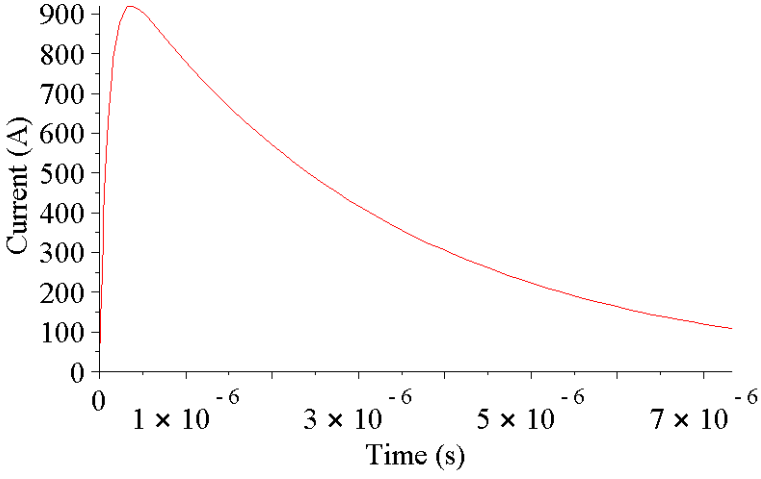

Twelve-volt solar panel array are extended from the spacecraft. The incoming voltage is then step-up by a standard DC-DC converter. This increases the voltage to 1,000 V. The electric flow charges the capacitors, C_1, C_2, …, C_n, and produces a DC arc in the thruster. The silicon-controlled rectifier (SCR) restricts the current when the gate (G) is off; when the gate is on, the current flows from the anode (A) to the cathode (K) of the SCR. The pulse generator triggers the SCR such that the thruster can run in quasi-steady state. It produces a +5 V pulse at 5.00 kHz. The model for the time-dependence of the total charge per pulse in the system is (Jahn, 1968; Horowitz and Hill, 2001):

$$L_{ind} \cdot \frac{d^2 Q_{charge}}{dt^2} + R_{res} \cdot \frac{dQ_{charge}(t)}{dt} + \frac{1}{C_{cap}} \cdot Q_{charge}(t) = V_{MPD}, \tag{7}$$

where $Q_{charge}(t)$ is the total charge in the capacitors at time t, L_{ind} is the internal inductance, R_{res} is the resistance, and C_{cap} is the capacitance. Normally, the internal resistance and inductance in capacitors are very low. There are 33 capacitors in the circuit; each of them has a capacitance of 100 nF and a rated voltage that of 1,000 V. Rather than obtaining large capacitors or high current power supply which cannot fit in a nanosatellite, low-energy capacitors are used to perform the quasi-steady state. This reduces the cost of the high-power system from $10,000 USD to less than $1,000 by using a step up DC voltage converter and low-energy capacitors.

In the mathematical model, it is assumed that the internal inductance and resistance to be 100 nH and 1 Ω, respectively. The maximum induced current from the capacitors is 920 A. The predicted result for the current versus time is shown in Figure 5.

4 Experiment

4.1 Methodology

Figure 6 shows the experimental setup for the MPD thruster. The compressed gases for this experiment are nitrogen, argon, and helium; the mixture compositions are 50% nitrogen – 50% helium and 50% argon – 50% helium. The total mass flow rate ranges between 200 μg/s and 600 μg/s. The gas flows continuously to reduce complications in the experiment using a volumetric flow gauge. In addition, before the capacitors discharge, the gas is ionised by DC discharge. The thruster is mounted on a pendulum and the experiment measures the force. The thermal vacuum chamber, number one in Figure 6, is 3 metres in length and 2 metres by diameter. In order to measure the performance using helium gas, the experiment is operated under medium vacuum, between 10–2 Torr and 1.0 Torr. Ingestion must be taken account in order to accurately measure the results:

$$\dot{V}_{ingested} = \frac{133.2}{4k_BT}\sqrt{\frac{8k_BT}{\pi m_i}} \cdot \frac{A_{active}}{4.479 \cdot 10^{23}} \cdot \tag{8}$$

The results were normalised and the back pressure has been taken into account using the modified thrust equation, from equation (3):

$$F_{thrust} = \dot{m} \cdot v_{ex} + A_e \left(P_e - P_{amb} \right), \tag{9}$$

where P_{amb} is the ambient pressure. Under the pure nitrogen and argon, the thruster is performed under high vacuum operating less than 10^{-5} Torr. The thruster operates for 10 seconds in order to stabilise the results of the thrust. No heat exchange between the chamber and the outside ambient environment; thus, the experiment is in thermal equilibrium (Goebel and Katz, 2008).

Figure 7 illustrates the electronic circuit for the MPD test. The function generator replaces the pulse generator as the trigger to simulate it. It produces the same +5 V pulse at 5.00 kHz as the pulse generator. The power supply, V_{MPD}, replaces the solar panels and the DC-DC converter for the experiment. This produces +1,000 VDC.

Figure 6 Experiment setup for the MPD thruster experiment (see online version for colours)

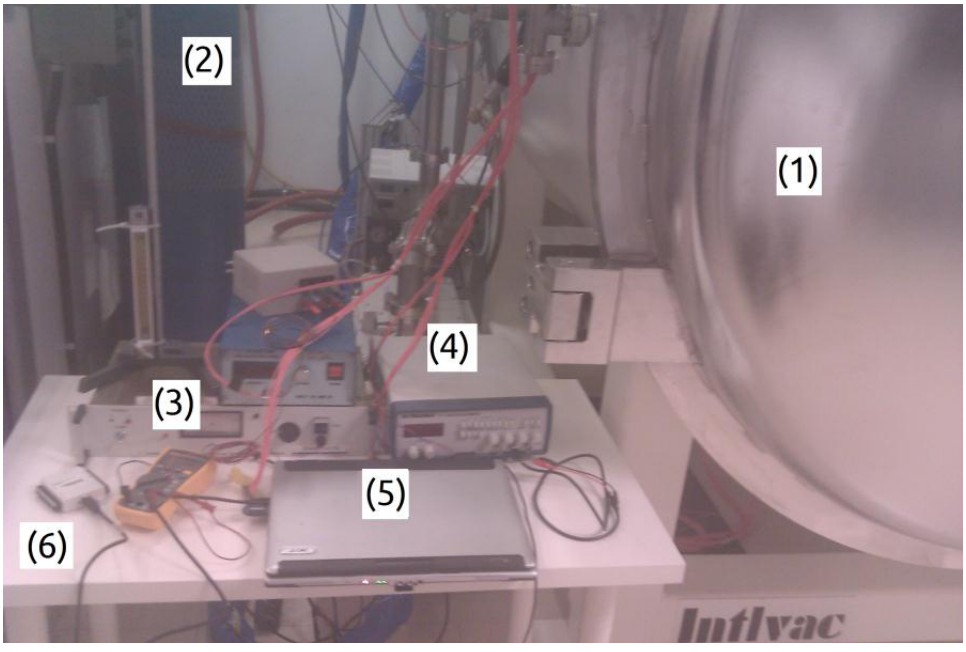

Notes: (1) – TVAC; (2) – compressed gases; (3) – DC power supply for the MPD circuit; (4) – function generator; (5) – computer for data acquisition; (6) – the data acquisition hardware.

Figure 7 Schematic of MPD thruster test in laboratory conditions

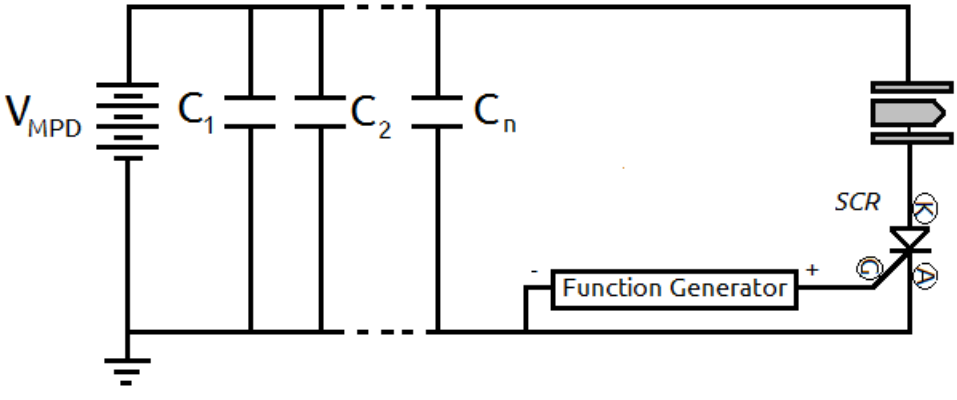

Figure 8 Cradle pendulum (see online version for colours)

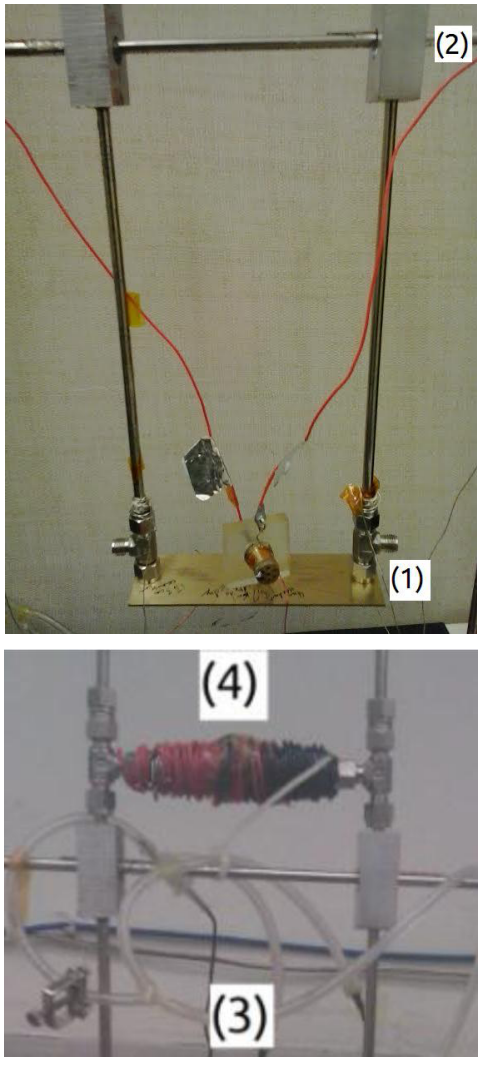

Notes: (1) – the cradle; (2) – the support structure; (3) – gas tubes; (4) – the counterweight.

Figure 8 shows the cradle system used in the experiment. The thruster is mounted on the cradle with a LED on top of the plasma thruster, not shown in the figure. The pivots resting on the knife edges ensure little or no friction is introduced to the pendulum. The gas tubes are mounted such that there would not be any interference between them and the pendulum. At the top of the pendulum, there is a counterweight to magnify the moment of the pendulum.

Figure 8 illustrates the pendulum-LED schematic of the experiment.

Figure 9 Pendulum-led schematic

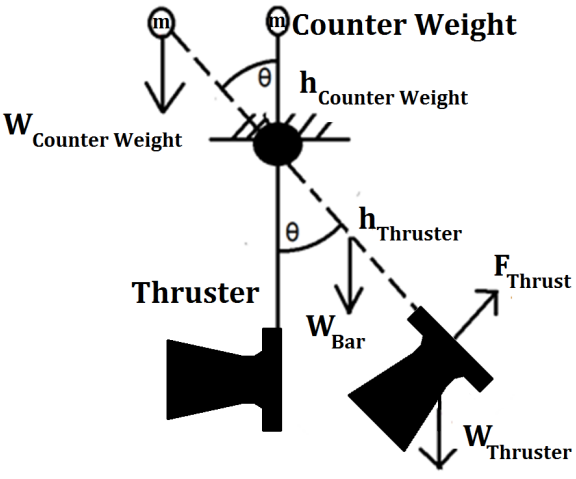

The total thrust from the engine is:

$$F_{Thrust} = \left(W_{Thruster} + W_{bar} - W_{counterweight} \cdot \frac{h_{counterweight}}{h_{Thruster}} \right) \cdot \sin(\theta), \tag{10}$$

where $h_{Counterweight}$ and $h_{Thruter}$ are the centre-of-mass heights of the counterweight and thruster, respectively. The weight of the bars, W_{bar}, is taken into account since it affects the results of the thrust. The counterweight, $W_{Counterweight}$, and its position determine the magnitude of the thrust.

Outside of the cradle, there is photodiode to read the input light intensity from the LED. The light spread of the LED is assumed to be a Gaussian distribution. The potential difference from the photodiode is recorded in the computer with a data acquisition (DAQ) card. The MATLAB program reads the voltage and converts it to force and specific impulse.

The LED readout needs to be calibrated for each experiment. To calibrate the readout, an accelerometer-based level is attached to the pendulum. The initial position of the pendulum is the zero, and at different angles, the LED readout results a certain voltage. After taking several readings, a linear regression line is fitted into the curve, yielding a linear voltage equation given the angle:

$$\theta = aV + b, \tag{11}$$

where a and b are the slope and the y-intercept resulting from the linear regression.

The performance is described by the modified specific impulse formula from equation (4):

$$I_{sp} = \left(\frac{1}{g} \cdot \frac{F_{thrust}}{\dot{m}} \right) \cdot (1 \pm C). \tag{12}$$

F_{thrust} is the measured thrust in the experiment. The constant C is the uncertainty constant in the experiment. The experimental errors include calibration error and the parasitic

forces in the pendulum. The uncertainty was calculated from the data collected in the experiment over time, which is 0.10.

Although the gas is flowing continuously, the thrust efficiency is calculated using a ratio of the kinetic energy pulse to the capacitors potential energy in which Δt is 200 μs (Guarducci et al., 2011):

$$\eta_t = \frac{\dot{m}\Delta t \cdot v_{ex}^2}{C_{cap} V_{volt}^2}. \tag{13}$$

The calculated results obtained from the experiment takes the mass bit, or the mass flow rate and the pulse time, at which electromagnetic propulsion occurs.

Figure 10 Specific impulse of argon-helium and nitrogen-helium gas mixtures in MPD thruster (see online version for colours)

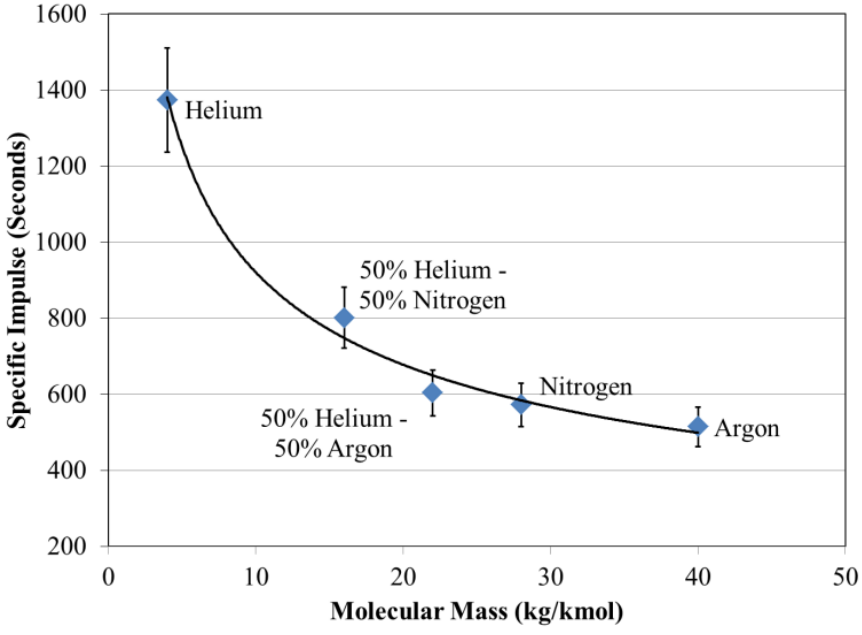

Notes: Mass flow rates – helium: 210 μg/s; 0.5 N_2-0.5 He: 460 μg/s; 0.5 Ar-0.5 He: 550 μg/s; Nitrogen: 400 μg/s; Argon: 570 μg/s.

Figure 10 shows the specific impulses of the MPD thruster using argon-helium and nitrogen-helium mixtures with the trendline that follows equation (2). The specific impulses in the figure normalise the varying mass flow rates. The specific impulses of all the gases are above 500 seconds. Figure 9 show that helium performed the best while argon performed the worst.

The 50% argon – 50% helium mixture has results comparable with argon. This means that there is marginal increase in the specific impulse when mixing with helium. The 50% nitrogen – 50% helium mixture shows a major improvement over the 50% argon – 50% helium mixture.

Table 1 Impulse bit [equation (6)]

Gas mixture	*Impulse bit (μN·s)*
Helium	2.84
50% N_2 – 50% He	6.29
50% Ar – 50% He	6.51
Nitrogen	5.05
Argon	5.75

Table 1 shows the impulse bit [equation (6)] of the gas mixtures. The time interval of all the calculated impulse bits is 200 μs. The argon-helium mixture shows the highest impulse bit. For spacecraft, the argon-helium mixture shows the highest change in momentum.

Table 2 Thrust efficiency [equation (11)]

Gas mixture	*Thrust efficiency*
Helium	15.3%
50% N_2 – 50% He	19.8%
50% Ar – 50% He	15.4%
Nitrogen	11.3%
Argon	11.6%

Table 2 shows the thrust efficiency [equation (11)] of the gas mixtures. The thruster efficiency table shows that nitrogen and argon have the lowest efficiencies. The pure helium and the 50% mixture show similar thrust efficiency. The helium – nitrogen mixture, notably, has the highest efficiency. The low efficiencies show that the amount of energy put in does not convert completely into usable thrust, possibly because of the energy transfer loss from the capacitors to the plasma for acceleration.

Table 3 Thrust-mass, thrust-power ratios

Gas mixture	*Dry mass ratio (mN/kg)*	*Thrust-power ratio (mN/W)*
Helium	7.10	33.1
50% N_2 – 50% He	15.72	39.7
50% Ar – 50% He	16.27	69.4
Nitrogen	12.63	68.0
Argon	14.38	95.2

Table 3 shows the dry thrust-mass and thrust-power ratios of the thruster using different gases and mixtures. It shows that 50% Ar – 50% He has the highest thrust-mass ratio of 16.27 mN/kg; the corresponding thrust-power ratio is 69.4 mN/W. This signifies this mixture provides the highest acceleration, which is useful for high-speed manoeuvres in deep-space missions.

5 Discussion

Table 4 shows the performance characteristics of the thrusters amongst the author, Paganucci, and Zeimer. Paganucci utilises a large power supply and operate in 50 ms pulses. The power output according to Paganucci is 1 MW, which results of a specific impulse of 2,750 seconds using Ar-He mixture (Paganucci and Andrenucci, 1995). Zeimer utilises a much lower power supply at 30 kW. The resulting specific impulse of Zeimer's thruster is 5,000 seconds under pure Ar (Ziemer and Choueiri, 1998). Stoute, this author, has an ultra-low power system in which capacitors are the primary factor for the performance of the thruster. At 20 W, the specific impulse is 600 seconds with Ar-He. Even though the specific impulse is only 600 seconds in comparison to the thrusters from Zeimer and Paganucci, the confinement of the circuit can be fitted in a nanosatellite (1 litre in volume). Paganucci also did work on scaling the thruster to 50 mm exhaust diameter and replaced the power system with 12.5 mF capacitors. The capacitor array is of higher capacitance than the 3.3 μF present in the MPD thruster. The result presents Paganucci's thruster has a maximum specific impulse of 1,200 seconds, more than double of the MPD thruster under argon operation (Andrenucci et al., 1991).

The MPD thruster at that low power only operates for manoeuvres and course correction. As stated in the introduction, this thruster is from a larger work where an ion thruster is present. The ion thruster operates as a sustainable thruster for deep missions, while the MPD thruster operates as an augmented thruster.

Table 4 Specific Impulse and efficiencies according to author

Author	*Stoute*	*Paganucci (Paganucci and Andrenucci, 1995)*	*Zeimer (Ziemer and Choueiri, 1998)*
Gas	Ar-He	Ar-He	Argon
Power (kW)	0.02	1,000	30
Capacitance (μF)	3.3	N/A	130
Energy per pulse (J)	1.65	N/A	4
Impulse bit (μN-s)	6.6	N/A	10.5
Specific impulse (seconds)	600	2,750	5,000
Thrust efficiency (%)	15.4	18	15

Source: Other data from Paganucci and Andrenucci (1995) and Ziemer and Choueiri (1998)

Table 5 Ionisation fraction [equation (5)]

Gas mixture	*Alfvèn's critical specific impulse (s)*	*Specific impulse from experiment (s)*	*Ionisation fraction (%)*
Helium	3,410	1,374	40%
50% N_2 – 50% He	1,628	801	49%
50% Ar – 50% He	1,232	603	49%
Nitrogen	1,116	572	51%
Argon	876	514	59%

Table 5 shows how much the gas was ionised by comparing the experimental specific impulses to the theoretical maximum specific impulse from Alfvèn's critical velocity.

The ionisation fraction shows how much of the gas has been ionised for electromagnetic propulsion. The results show that helium has the lowest ionisation fraction at 40% while argon has the highest at 59%. Given that the results of the ionisation fraction were derived from using the experimental specific impulse and the theoretical Alfvèn's critical velocity, the results show that the mixing the gases increase the ionisation fraction.

6 Conclusions

The N_2-He gas mixture shows a promising result among the thrust efficiency in comparison to the rest of the gases. The high efficiency indicates the thruster is utilising the propellant effectively. The impulse bit of the N_2-He mixture is comparable to the Ar-He mixture; the difference between the two mixtures is 2.2 μN·s. Comparing to the pure mixtures, the difference in impulse bit ranges between 8.5% (argon) and 55% (helium). The delta-V and kinetic power of the N_2-He mixture in a 10 kg spacecraft with 5 kg of fuel are 3182 $m \cdot s^{-1}$ and 15.4 W respectively.

Acknowledgements

This research paper has been supported from my supervisor Dr. Brendan M. Quine. In addition, this experiment was funded in part by the Natural Science and Engineering Research Council, Ontario Centre of Excellence, York University, Thoth Technology Inc. and Discovery Channel Canada.

References

Andrenucci, M., Paganucci, F., Frazzetta, M., La Motta, G. and Schianchi, G. (1991) 'Scale effects on the performance of MPD thrusters', in *22nd International Electric Propulsion Conference*, Viareggio, p.10.

Chang Díaz, F.R. et al. (1999) *The Development of the VASIMR Engine*, Torino, 13 September.

Domonkos, M.T., Gallimore, A.D., Myers, R.M. and Thompson, E. (1995) 'Preliminary pulsed MPD thruster performance', in *31st Joint Propulsion Conference*, San Diego, p.8.

Goebel, D.M. and Katz, I. (2008) *Fundamentals of Electric Propulsion: Ion and Hall Thrusters*, Wiley, New Jersey.

Guarducci, F., Paccani, G. and Lehnert, J. (2011) *Quasi steady MPD performance analysis*, Vol. 68.

Horowitz, P. and Hill, W. (2001) *The Art of Electronics*, The Press Syndicate of the University of Cambridge, Cambridge, UK.

Jahn, R.G. (1968) *Physics of Electric Propulsion*, McGraw-Hill, New York.

Martinez-Sanchez, M. (2004) *Space Propulsion*, Massachusettes Institute of Technology, Boston.

Paganucci, F. and Andrenucci, M. (1995) 'MPD Thruster performance using pure gases and mixtures as propellant', in *Joint Propulsion Conference and Exhibit*, San Diego, p.12.

Stoute, C.A.B. (2013) *Hybrid Electric Thruster using Gas Mixtures*, York University, Toronto.

Sutton, G.P. and Biblarz, O. (2010) *Rocket Propulsion Elements*, Wiley, New Jersey.

Ziemer, J.K. and Choueiri, E.Y. (1998) 'Dimensionless performance model for gas-fed pulsed plasma thrusters', in *Joint Propulsion Conference*, Cleveland, p.13.

Nomenclature

E	Electric field (V/m)
F_{nozzle}	Nozzle thrust (N)
$F_{Maecker}$	Magnetoplasmadynamic thrust (N)
F_{Thrst}	Overall thrust (N)
γ	Heat capacity ratio
I	Current (A)
I_{bit}	Impulse bit (Ns)
I_{sp}	Specific Impulse (s)
J	Current density (A/m^2)
g_0	Earth's gravitational constant (9.806 m/s^2)
$\dot{m}$	Mass flow rate (kg/s)
M	Atomic mass (kg/kmol)
μ_0	Permeability of free space ($4\pi \cdot 10^{-7}$ H/m)
P_a	Atmospheric pressure (Pa)
P_e	Exhaust pressure (Pa)
ρ_q	Charge density (C/m^3)
R	Universal gas constant ($J \cdot kmol^{-1} \cdot K^{-1}$)
r_a	Radius of anode (m)
r_c	Radius of cathode (m)
Δt	Period of pulse (s)
v_{ex}	Exhaust velocity (m/s)